Loop-Tryptophan Human Purine Nucleoside Phosphorylase Reveals Submillisecond Protein Dynamics[†]

Mahmoud Ghanem,[‡] Nickolay Zhadin, Robert Callender, and Vern L. Schramm*

Department of Biochemistry, Albert Einstein College of Medicine, Bronx, New York 10461

Received December 22, 2008; Revised Manuscript Received February 3, 2009

ABSTRACT: Human PNP is a homotrimer containing three tryptophan residues at positions 16, 94, and 178, all remote from the catalytic site. The catalytic sites of PNP are located near the subunit−subunit interfaces where F159 is a catalytic site residue donated from an adjacent subunit. F159 covers the top (β) surface of the ribosyl group at the catalytic site. QM/MM calculations of human PNP have shown that F159 is the center of the most mobile region of the protein providing access to the substrate in the active site. F159 is also the key residue in a cluster of hydrophobic residues that shield catalytic site ligands from bulk solvent. Trp-free human PNP (Leuko-PNP) was previously engineered by replacing the three Trp residues of native PNP with Tyr. From this active construct, a single Trp residue was placed in the catalytic site loop (F159W-Leuko-PNP) as a reporter group for the ribosyl region of the catalytic site. The F159W-Leuko-PNP fluorescence is red shifted compared to native PNP, suggesting a solvent-exposed Trp residue. Upon ligand binding (hypoxanthine), the 3-fold fluorescence quench confirms conformational packing of the catalytic site pocket hydrophobic cluster. F159W-Leuko-PNP has an on-enzyme thermodynamic equilibrium constant (K_{eq}) near unity in the temperature range between 20 and 30 °C and nonzero enthalpic components, making it suitable for laser-induced T-jump analyses. T-jump relaxation kinetics of F159W-Leuko-PNP in equilibrium with substrates and/or products indicate the conformational equilibria of at least two ternary complex intermediates in the nano- to millisecond time scale (1000−10000 s^{-1}) that equilibrate prior to the slower chemical step (~200 s^{-1}). F159W-Leuko-PNP provides a novel protein platform to investigate the protein conformational dynamics occurring prior to transition state formation.

Human purine nucleoside phosphorylase (PNP)[1] is a homotrimer that catalyzes the reversible phosphorolysis of 6-oxopurine nucleosides and deoxynucleosides to the corresponding purine bases and α-D-(deoxy)ribose 1-phosphate (*1*−*6*) (Scheme 1). The genetic deficiency of PNP leads to a specific T-cell immune deficiency (*1*). Transition-state analogue inhibitors of PNP provide potential therapies for T-cell cancers and autoimmune diseases including rheumatoid arthritis, psoriasis, tissue transplant rejection, and multiple sclerosis (*7*−*9*). Crystal structures of PNP complexed with substrate, substrate analogues, or transition-state analogues have defined the active site residues in contact with the purine nucleoside and the phosphate nucleophile (Figure 1) (*10*−*13*). Human PNP is a homotrimer containing three tryptophan residues at positions 16, 94, and 178, which are all remote from the catalytic site (Figure 1). The catalytic sites of PNP are located near the subunit−subunit interfaces where F159 is a catalytic site residue donated from an adjacent subunit (Figure 1). It is the only residue from the neighboring subunit which participates in catalytic site contacts by covering the top surface of the ribosyl group of bound purine nucleoside (Figure 1). QM/MM calculations of human PNP have shown that F159 is the center of the most mobile region of the protein (*4, 14*). Calculations also reveal correlated motions between residues 57−65 of subunit A (a phosphate-binding loop) and residues 155−160 of subunit C (the F159 loop) (*14*). These loops interact through the subunit interface. Interestingly, F159 is the key residue among a cluster of residues (F159, H257, F200, and Y88) that shield ligands in the catalytic pocket from bulk solvent (Figure 1) (*14*).

Atomic motion on the femtosecond to millisecond time scale is important for enzymatic catalysis (*15, 16*) (Table 1). For example, the steady-state turnover for PNP is ~40 s^{-1} (25 ms), the chemical step is ~200 s^{-1}, reaction coordinate motion is ~100 fs, and the lifetime of the transition state is ~10 fs (*17*) (Table 1). Therefore, the catalytic cycle takes 2500000000000 times longer than the transition-state lifetime (*18*). Computationally, specific, fast protein dynamic motions can be correlated with transition-state formation. However, proteins also undergo conformational changes in the nanosecond to millisecond time scale to bind reactants and arrange into a form suitable for transition-state formation. A major problem has been experimental access to the broad and often uncoupled time scales to validate the dynamic modes at all stages of the reaction coordinate. During the past decade, efforts on dynamic contributions to enzymatic catalysis have focused on computational and

[†] Supported by NIH Research Grants GM41916 and GM068036.

* Corresponding author. E-mail: vern@aecom.yu.edu. Telephone: (718) 430-2813. Fax: 718-430-8565.

[‡] Faculty of Veterinary Medicine, Cairo University, Egypt.

[1] Abbreviations: PNP, native human purine nucleoside phosphorylase; Leuko-PNP, a tryptophan-free mutant PNP with all tryptophan residues (W16, W94, and W178) replaced with tyrosine residues; F159W-Leuko-PNP, Leuko-PNP with tyrosine 159 replaced by tryptophan.

10.1021/bi802339c CCC: $40.75
Published on Web 02/03/2009

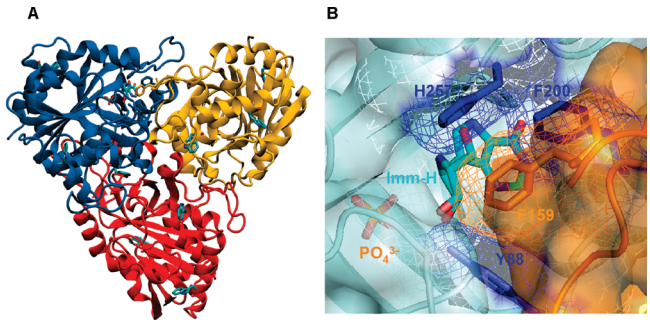

FIGURE 1: (A) Trimeric crystal structure of human PNP in complex with immucillin-H (Imm-H) and phosphate, with highlighted remote tryptophan residues (PDB 1RR6). (B) A close-up space-filling view of the catalytic site contact residues at the subunit−subunit interface.

experimental validation of protein conformational changes in the nanosecond to millisecond time scale with approaches including (1) NMR (*19*−*26*), (2) infrared laser-induced T-jump perturbation (*27*−*33*), and (3) more recently TPS (transition path sampling) approaches (*17, 34*−*37*).

Laser-induced temperature-jump spectroscopy was employed to characterize the conformational dynamics of selective regions of the PNP catalytic site that lead to a catalytically competent ternary complex. A single Trp mutant of PNP provides a reporter group to probe the motions of the catalytic site F159 loop near the ribosyl region of bound reactants. Trp-free PNP (Leuko-PNP) previously allowed collection of T-jump data on guanine fluorescence spectra, free of native PNP chromogenic effects (*38*). From this construct, the single Trp residue (F159W-Leuko-PNP) described here was used to investigate kinetic, fluorescent, and dynamic properties associated with catalysis for this region of the catalytic site.

MATERIALS AND METHODS

Site-Directed Mutagenesis. A QuikChange site-directed mutagenesis kit (Stratagene) was used to prepare the loop-tryptophan PNP (F159W-Leuko-PNP), in which the phenylalanine residue (F159) was replaced with tryptophan. The method was used according to the manufacturer's instructions, with the Leuko-PNP gene inserted into pCRT7/NT-TOPO (*38*) as a template and F159Wf 5′-GGTTTGGAGATCGTTGGCCTGCCATGTCTGATGC-3′ and F159Wr 5′-GGCATCAGACATGGCAGGCCAACGATCTCCAAACCTTTC-3′ oligonucleotides as forward (f) and reverse (r) primers, respectively (underlined letters indicate mismatches). The DNA sequence of the mutant enzyme was confirmed, and the plasmid was transformed into *Escherichia coli* strain BL21(DE3)pLysS competent cells (Invitrogen).

Expression and Purification of F159W-Leuko-PNP. F159W-Leuko-PNP was expressed and purified to homogeneity as judged by SDS−PAGE using the same procedure used previously for the purification of the native and Leuko-PNP (*38, 39*).

Preparation of Hypoxanthine-free F159W-Leuko-PNP. Similar to native and Leuko-PNP, F159W-Leuko-PNP as purified in 20 mM Tris-HCl, pH 7.4, contained tightly bound hypoxanthine in a stoichiometry of ∼0.7 to 1 per enzyme monomer, indicating that at least two out of the three active sites of the enzyme trimer are occupied with hypoxanthine (*38*). Incubation of the enzymes in 100 mM $(NH_4)_2SO_4$ in the presence of 10% charcoal (w/v) for 5 min followed by centrifugation and filtration of the enzyme resulted in the preparation of phosphate and hypoxanthine-free F159W-Leuko-PNP as indicated by reverse-phase HPLC and UV spectral analysis.

Enzyme Assays. Activity assay for F159W-Leuko-PNP with inosine as a substrate was carried out by monitoring the conversion of hypoxanthine to uric acid (ε_{293} = 12.9 mM^{-1} cm^{-1}) (*40*) in a coupled assay containing 60 milliunits of xanthine oxidase and variable concentrations of inosine, in 50 mM KH_2PO_4, pH 7.4 at 25 °C (*41*). The slow onset of inhibition was measured following the addition of enzyme to complete assay mixtures at ∼8 mM inosine and various inhibitor concentrations (*42, 43*). Inhibitor concentrations were determined spectrophotometrically using the published millimolar extinction coefficient of 9.54 at 261 nm at pH 7 for 9-deazainosine (ImmH-based inhibitors) (*43*−*45*). Enzyme (0.2−0.5 nM final concentration) was added to assay mixtures followed by monitoring of product formation. Rates were monitored for 1−2 h both to determine the initial reaction rate and to determine if slow-onset inhibition occurred.

Fluorometric Titration of F159W-Leuko-PNP. The fluorescence emission spectra (λ_{ex} = 295 nm, 2.5 nm slit width, and 10 mm path length) of free or ligand-bound F159W-Leuko-PNP were acquired using a FluroMax-3 spectrofluorometer thermostated at 25 °C. The dissociation constants for different ligands were obtained from the fluorometric titrations of the hypoxanthine-free PNPs (3 μM) with different ligands (hypoxanthine in the presence and the absence of 50 mM phosphate and inosine in the presence and the absence of sulfate and/or phosphate) at pH 7.4. Typically, during titrations, the dilution does not exceed 10%, and all of the fluorescence emission spectra were corrected for dilution. Inosine and hypoxanthine stock solutions were prepared fresh prior to each titration, and their concentrations were determined spectrophotometrically using the published millimolar extinction coefficients of 12.3 mM^{-1} cm^{-1} at 249 nm and 10.7 mM^{-1} cm^{-1} at 250 nm at pH 7 for inosine and hypoxanthine, respectively (*46*).

Stopped-Flow Fluorescence and Quench-Flow Kinetics. The temperature dependence for the forward and the reverse single turnover catalysis of F159W-Leuko-PNP with inosine and native PNP with guanosine as substrates was determined using an KinTek SF-MiniMixer stopped-flow attached to a FluoroMax-3 spectrofluorometer equipped with a thermostated water bath, by following the quenching (forward reaction for F159W-Leuko-PNP with inosine or reverse reaction for native PNP with guanine and ribose 1-phosphate) or increase (reverse reaction for F159W-Leuko-PNP with hypoxanthine and ribose 1-phosphate or forward reaction for native PNP with guanosine) of fluorescence intensity above 300 nm upon excitation at 295 nm (10−20 nm slit widths, 10 mm path length). The forward single turnover reactions involved mixing equal volumes of ∼5−6 μM enzyme in 100 mM KH_2PO_4, pH 7.4, against saturated substrate solutions (∼2−3 mM inosine for F159W-Leuko-PNP or guanosine for native PNP) in the same buffer, in the temperature range between 1 and 20 °C. The reverse single turnover reactions involved mixing equal volumes of ∼5−6 μM enzyme containing ∼2 mM hypoxanthine for F159W-Leuko-PNP or

Scheme 1

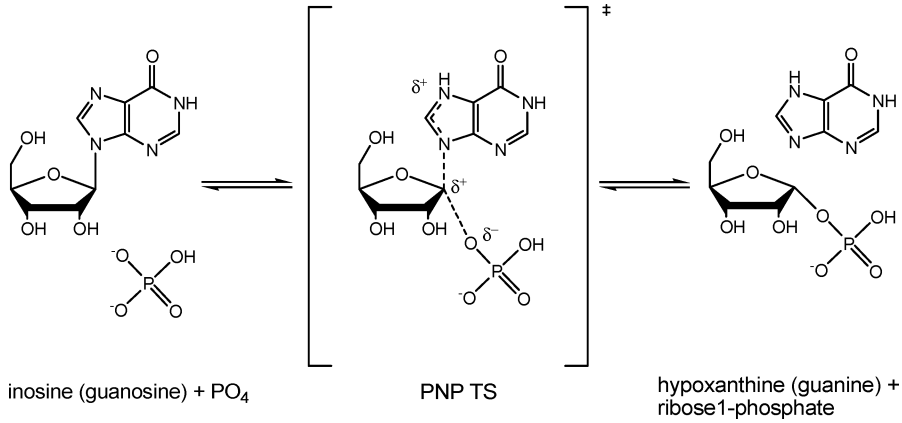

Table 1: Time Constants of Molecular Dynamics, Protein Motion, and Catalysis[a]

Time		sec			
	s	1			common k_{cat} range
	ms	10^{-1}			
		10^{-2}		k_{cat} PNP	
		10^{-3}	flap opening TIM	k_{chem} PNP	
	μs	10^{-4}	rate O_2 Hb to deoxy Hb	loop motion PNP	
		10^{-5}	flap closing OPRTase and PTPase		domain motion in protein
		10^{-6}			
	ns	10^{-7}		substrate/ligand binding PNP[b]	
		10^{-8}			rotation/translation for NACs catalytic site capture limit[a]
		10^{-9}			
	ps	10^{-10}			
		10^{-11}	H_2O diffuses two diameters		
		10^{-12}	light travels 0.3 mm		
	fs	10^{-13}			
		10^{-14}	bond vibration; TS lifetime	TS PNP[c]	
		10^{-15}			

[a] Modified from ref *18*. [b] From ref *38*. [c] From ref *17*.

guanine for native PNP in 20 mM Tris-HCl, pH 7.4, against 2 mM ribose 1-phosphate in the same buffer, in the temperature range between 1 and 20 °C. Data points (20−100) were recorded over the course of each reaction (0.02−0.1 s), and at least three runs were averaged for each temperature. The forward and reverse single turnover rates at different temperatures were determined by fitting the stopped-flow traces into a single exponential equation using the software provided by the manufacturer. The reverse single turnover catalysis of F159W-Leuko-PNP with hypoxanthine and ribose 1-phosphate was also independently determined using KinTek RQF-3 rapid quench-flow at room temperature. The reverse single turnover reaction involved rapid mixing (0.002−3 s) of equal volumes of 150 μM F159W-Leuko-PNP containing ~1 mM hypoxanthine in 20 mM Tris-HCl, pH 7.4, against 5 mM ribose 1-phosphate in the same buffer, followed by automatic acid quenching (0.6 N HCl) and collection of the quenched reactions. The ratio of hypoxanthine to inosine was then quantified using reverse-phase HPLC. The reverse single turnover rate for F159W-Leuko-PNP was determined by plotting the inosine formed as a function of mixing time and fitting the data to a single exponential equation (eq 2). The temperature dependence for the rates of hypoxanthine binding to F159W-Leuko-PNP was also determined using stopped-flow fluorometry as described above. The quench of fluorescence intensity above 300 nm upon excitation at 295 nm (20 nm slit widths, 10 mm path length) was followed. The reactions involved mixing equal volumes of ~6 μM enzyme in 100 mM KH_2PO_4, pH 7.4, against saturated ligand solutions (51 or 70 μM for hypoxanthine) in the same buffer, in the temperature range between 1 and 25 °C. Data points (20−100) were recorded over the course of each reaction (0.02−0.1 s), and at least three runs were averaged for each temperature. The rates of hypoxanthine binding to F159W-Leuko-PNP at different temperatures were determined by fitting the kinetic data to a single exponential equation using the software provided by the manufacturer.

T-Jump Relaxation Kinetics of F159W-Leuko-PNP. The laser-induced T-jump relaxation kinetics for equilibrated systems with the single Trp-reporter-PNP, inosine, phosphate, hypoxanthine, and ribose 1-phosphate or for the ternary complex of PNP, hypoxanthine, and phosphate were determined by methods described previously (*28, 29, 31, 33, 38*). Temperature jumps were induced by a pulse of infrared light (1.56 μm wavelength, 90−120 mJ energy, 1.5 mm diameter spot on the sample, 0.5 mm path length), generated by stimulated Raman shifting the fundamental emission (1.064

Scheme 2

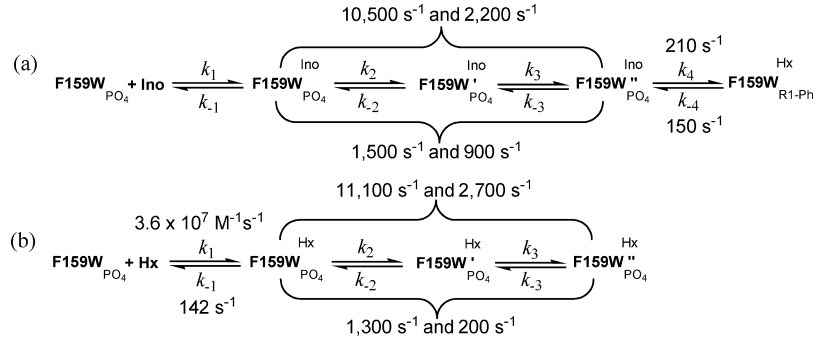

μm) of a Powerlite 7010 Q-switched Nd:YAG laser (Continuum, Santa Clara, CA), operating at 2 Hz, in a 1 m long cell filled with deuterium gas at 650 psi. Water absorbs the laser energy, and the temperature of the exposed volume increases in approximately 10 ns. The size of the T-jump was calibrated using the change of water IR absorption with temperature. Typical T-jump values ranged from 6.5 to 8.5 °C. Diffusion of heat out of the interaction volume proceeds with a time constant of approximately 35 ms. Hence, the apparatus generated a T-jump within 10 ns that remained constant for approximately 10 ms.

The fluorescence excitation of the tryptophan fluorophore involved irradiation by emission lines near 300 nm from an Innova 200-25/5 argon ion laser (Coherent, Palo Alto, CA). To avoid photodamage, the excitation light was modulated using a shutter that allowed 19 ms exposure for every T-jump pulse. The power of the excitation beam was 3−5 mW. The incident excitation beam is focused onto a 0.3 mm diameter spot on the sample, in the center of the heated spot. Tryptophan fluorescence emission, detected at 50° to the excitation beam, was passed through a narrow band filter (340 ± 12 nm) and was monitored using a R4220P photomultiplier tube (Hamamatsu, Bridgewater, NJ). Data were digitized with a CS82G data acquisition board (Gage Applied Technologies, Montreal, Quebec, Canada) at 1 GS/s sampling rate. Overall temporal resolution of the system is about 20 ns. A background signal obtained without fluorescence excitation was measured separately and subtracted from the kinetic data. A program written in LabVIEW (National Instruments, Austin, TX) was used for instrument control and data collection. Data were normalized to the average fluorescence intensity taken before the T-jump.

Typically, T-jump relaxation profiles were obtained by subjecting the sample containing ~28 μM F159W-Leuko-PNP in 50 mM KH_2PO_4, pH 7.4, and variable concentrations of either inosine (13−800 μM) or hypoxanthine (5.7−798 μM) to a laser-induced temperature jump (from 10 to 18, 20 to 27, and 25 to 32 °C) every 500 ms. The relaxation is monitored using fluorescence for the first 14 ms after the T-jump; once 300 ms has elapsed, the sample has relaxed to its original temperature, allowing the T-jump to be repeated. Each relaxation curve contains data from 3600 temperature jumps on the same sample. Curve fitting was done with OriginPro (OriginLab, Northampton, MA) software. The small spurious signals that sometimes appear in the relaxation spectra between 1 and 20 μs are due to transient microbubble formation. In those cases, curve fitting started at 20 or 30 μs. The uncertainties in the reported values of relaxation rates were determined from the fitting parameters.

Data Analysis. The dissociation constants for the binding of hypoxanthine to F159W-Leuko-PNP were determined by fitting the fluorometric titrations data to eq 1, where F_0, F_{EL}, and $F_{EL\infty}$ are the intrinsic fluorescence of the free enzyme, ligand-bound enzyme, and enzyme at saturating ligand concentration, respectively, [L] is the total ligand concentration, and K_d is the dissociation constant of the enzyme−ligand complex. The single turnover rates (forward or reverse) at different temperatures were determined by fitting the stopped-flow traces into the equation for single exponential decay (eq 2), where k_{obs} represents the first-order rate constant of the chemical step, t is time, F_t is the fluorescence emission intensity above 295 nm, A is the amplitude of the total change, and F_∞ is the fluorescence intensity at infinite time. The temperature dependence of the single turnover rates (k) was determined by fitting the data with the Arrhenius and the Eyring equations (eqs 3 and 4, respectively), where k_B and h are the Boltzmann and Planck constants, respectively, A is the preexponential factor, E_a is the energy of activation, R is the gas constant (8.31 J mol^{-1} K^{-1}), and T is the temperature in kelvin. The enthalpy of activation ($\Delta H^{\ddagger}$) is calculated from the slope of the plots, whereas the entropy ($\Delta S^{\ddagger}$) is calculated from the y-intercept of the plots. The microscopic rate constants (k_2, k_{-2}, k_3, and k_{-3}) of the conformational changes for F159W-leuko-PNP equilibrated systems (Scheme 2) were obtained directly by fitting the T-jump relaxation times τ_2^{-1} and τ_3^{-1} to eqs 5 and 6 (*47*), respectively.

$$F_{EL} = \left(\frac{F_{EL\infty}[L]}{K_d + [L]}\right) + F_0 \quad (1)$$

$$F_t = A \exp(-k_{obs}t) + F_\infty \quad (2)$$

$$\ln(k) = \ln A - [E_a/RT] \quad (3)$$

$$\ln(k/T) = \ln(k_B/h) + \Delta S^{\ddagger}/R - \Delta H^{\ddagger}/RT \quad (4)$$

$$\tau_2^{-1} = k_2 \frac{k_1([F159W] + [Ino/Hx])_{free}}{k_1([F159W] + [Ino/Hx])_{free} + k_{-1}} + k_{-2} \quad (5)$$

$$\tau_3^{-1} = k_3 \frac{k_1([F159W] + [Ino/Hx])_{free} k_2}{k_1([F159W] + [Ino/Hx])_{free} k_2 + k_1([F159W] + [Ino/Hx])_{free} + k_{-1} + k_{-2}} + k_{-3} \quad (6)$$

RESULTS AND DISCUSSION

Expression and Purification of F159W-Leuko-PNP. F159W-Leuko-PNP was expressed and purified to homogeneity as

Table 2: Comparison of Steady-State Kinetic Constants and Inhibition Constants for F159W-Leuko-, Native, and Leuko-PNPs with Inosine as Substrates and with Immucillin Inhibitors[a]

parameter	F159W-Leuko-PNP	Leuko-PNP[b]	native PNP[b]
Inosine as a Substrate			
k_{cat}, s^{-1}	22 ± 1	36 ± 1	44 ± 2
K_m, μM	422 ± 30	50 ± 3	71 ± 8
k_{cat}/K_m, M^{-1} s^{-1}	$(5.2 \pm 0.4) \times 10^4$	$(7.2 \pm 0.4) \times 10^5$	$(6.2 \pm 0.7) \times 10^5$
ImmH as an Inhibitor[c]			
K_i*,[c] pM	2100 ± 60	134 ± 12	88 ± 3
DADMe-ImmH as an Inhibitor[c]			
K_i*, pM	60 ± 2	12 ± 3	8.5 ± 0.3

[a] Enzymatic assays with either substrates or inhibitors were performed in 50 mM KH_2PO_4, pH 7.4, at 25 °C. [b] From ref *38*. [c] DADMe-ImmH, 4′-deaza-1′-aza-2′-deoxy-1′-(9-methylene)-immucillin-H; ImmH, immucillin-H; K_i*, slow-onset tight binding constant for inhibitors.

judged by SDS−PAGE using the same procedure described previously for the purification of native or Leuko-PNP (*38, 39*). Approximately 100 mg of pure enzyme was obtained from 1 L of Luria−Bertani culture medium. Similar to native and Leuko-PNP, the incubation of F159W-Leuko-PNP in 100 mM $(NH_4)_2SO_4$ (a nonreactive analogue of phosphate) in the presence of activated charcoal removes the tightly bound hypoxanthine. This confirms the role of inorganic phosphate, sulfate, or arsenate in assisting hypoxanthine release from the tightly bound PNP−hypoxanthine complex (*48*).

Steady-State Kinetic and Slow Onset Inhibition Properties. The steady-state kinetic parameters of F159W-Leuko-PNP were determined with inosine as substrate and immucillin inhibitors and compared to those for the native and Trp-free enzymes (Table 2). The single Trp mutant PNP has k_{cat} and K_m altered by ~2- and 7-fold, respectively (Table 2). The overall catalytic efficiency of F159W-Leuko-PNP is therefore reduced by ~14-fold relative to native and Leuko-PNPs (Table 2). The binding affinity of transition-state analogues to F159W-Leuko-PNP is reduced by ~20- and 10-fold for ImmH and DADMe-ImmH (the preferred transition-state analogue for human PNP (*39*)), respectively (Table 2). Differences in K_m values and the dissociation constants for transition-state analogues suggest differences in transition-state structure as recently established for PNPs with mutations remote from the catalytic sites (*49*−*51*). Despite the four amino acid substitutions, F159W-Leuko-PNP remains active and provides a useful spectroscopic probe to study the fluorescent and the dynamic properties of the catalytic site.

Fluorescence Properties of F159W-Leuko-PNP. The intrinsic fluorescence properties of F159W-Leuko-PNP were significantly different from those for native or Leuko-PNP upon excitation at 295 nm (Figure 2). While Leuko-PNP has no fluorescence emission maxima and native PNP (three Trp residues) has emission maximum centered at 340 nm (*38*), F159W-Leuko-PNP showed an 10 nm shift of the emission maximum (λ_{max} centered at 350 nm) with similar intrinsic fluorescence intensity relative to native PNP (Figure 2). Fluorometric titration of F159W-Leuko-PNP with hypoxanthine in the absence or presence of phosphate (50 mM KH_2PO_4) showed ~3-fold decrease in fluorescence intensity without a significant shift of the emission maximum (Figure 2A,B). Titration data fitted to eq 1 gave K_d values of 3.3 ± 0.2 μM and 16 ± 2 μM for hypoxanthine in the absence and the presence of phosphate, respectively (Figure 2A,B). No cooperative interactions are observed as the three catalytic sites are filled. Fluorometric titration of F159W-Leuko-PNP with its substrate, inosine (up to ~100 μM), in the absence or presence of inorganic sulfate (a nonreactive analogue of phosphate, up to 3 mM) does not alter the fluorescence emission spectrum of the enzyme (Figure 2C). Upon the addition of phosphate to the enzyme−inosine complex, hypoxanthine is generated and fluorescence is quenched (Figure 2C). The red shift of the emission spectrum of the free enzyme suggests a solvent-exposed Trp residue in unliganded F159W-Leuko-PNP (*52, 53*). In native PNP the Trp residues are embedded in the hydrophobic core (*38, 52, 53*). Upon hypoxanthine binding to the enzyme active site, the 3-fold quenching in fluorescence intensity confirms F159 as a key residue in the conformational packing of the hydrophobic cluster (F159, H257, Y88, and F200) in the catalytic pocket (Figure 1) (*14*). The fluorescent properties of F159W-Leuko-PNP provide a catalytic site reporter with large

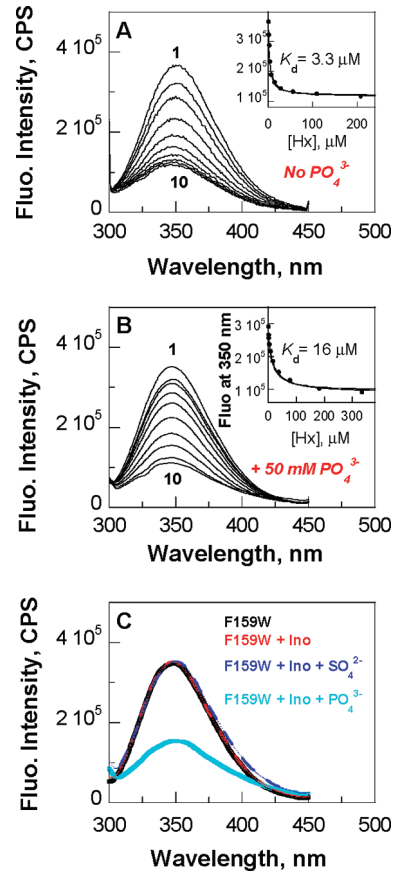

FIGURE 2: Ligand and substrate binding to F159W-Leuko-PNP. Fluorescence emission spectra (λ_{ex} = 295 nm) of F159W-Leuko-PNP in the absence (panel A) and the presence (panel B) of phosphate during the fluorometric titration of hypoxanthine in a concentration range between zero (panels A and B, curves 1) and 208 μM (panel A, curve 10) or 333 μM (panel B, curve 10). Insets: Fluorescence emission intensity values (●) at 350 nm as a function of hypoxanthine (panels A and B); the curves are fits of the data to eq 1. Panel C: Fluorescence emission spectra (λ_{ex} = 295 nm) of F159W-Leuko-PNP before (black curve) and after the titration of ~100 μM inosine (red curve), then the titration of up to 3 mM sulfate (blue curve), and finally after the titration of up to 12 mM phosphate (light blue curve). Fluorescence emission spectra were recorded at enzyme concentrations of ~3 μM in 20 mM Tris-HCl (panels A and C) or 50 mM KH_2PO_4 (panel B), pH 7.4, at 25 °C.

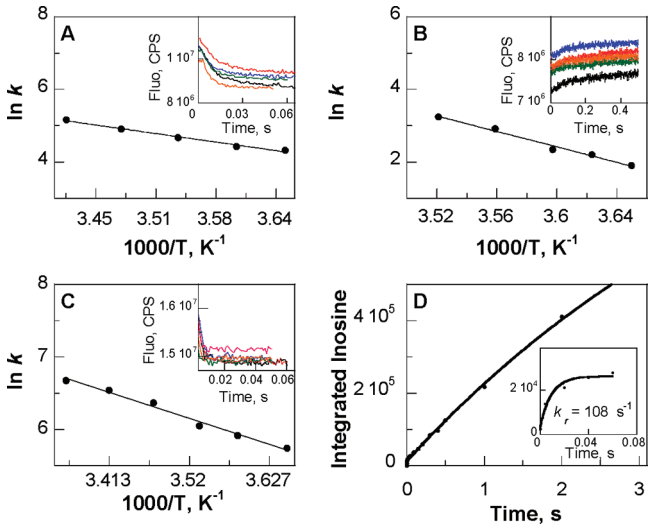

FIGURE 3: Pre-steady-state kinetics. Panels A−C: Arrhenius plots for the temperature dependences of the forward (panel A) and the reverse (panel B) single turnover rates (k_4 and k_{-4}) and hypoxanthine association rates (k_{on}) (panel C) for F159W-Leuko-PNP; data were fit to eq 3. Insets: Stopped-flow traces of fluorescence decrease (panels A and C) or increase (panel B) as a function of time due to the formation/association or removal of hypoxanthine, respectively, in the temperature range from 1 to 25 °C (black, red, blue, green, orange, and pink curves were recorded at 1, 5, 10, 15, and 20 °C, respectively, in panel A, 1, 3, 5, 7, and 11 °C, respectively, in panel B, or 1, 6, 10, 15, 20, and 25 °C, respectively, in panel C); traces were fit to eq 2. Panel D: Integrated amount of inosine (●) formed during the reverse reaction of F159W-Leuko-PNP as a function of mixing time. Acid quenching of the reaction as indicated in the quench-flow kinetics section in Materials and Methods was followed by inosine analysis. Data were fit to eq 2. Inset: A close-up view for the integrated amount of inosine formed during the first 0.05 s of the reverse reaction.

fluorescence changes as a function of catalysis and upon ligand binding. F159W-Leuko-PNP can also be employed to study the dynamic chemical equilibrium for hypoxanthine binding and hypoxanthine ↔ inosine equilibrium perturbation at the catalytic site of PNP by using the T-jump fluorescence relaxation approach, provided that the reaction exhibits a nonzero enthalpy.

Pre-Steady-State and On-Enzyme Equilibrium Kinetics. Stopped-flow fluorescence and/or quench-flow studies for the formation or the removal of hypoxanthine as a function of temperature and at saturated substrate concentrations provide the forward ($k_{(chem)f}$) and the reverse ($k_{(chem)r}$) single turnover catalytic rates for F159W-Leuko-PNP (Figure 3 and Table 3). For comparison, the forward and reverse single turnover catalytic rates for native PNP were determined for the formation or the removal of guanine (Table 3), using the unique property that guanine bound to native PNP is fluorescent. Free guanine and hypoxanthine, guanosine, or inosine on or off enzyme are very weakly fluorescent at neutral pH (*38, 49, 54*). As shown in Table 3, the single turnover rates for the forward and the reverse chemical reaction for F159W-Leuko-PNP with inosine−hypoxanthine and native PNP with guanine−guanosine (in the temperature between 1 and 20 °C) or extrapolated (above 20 °C) from the Arrhenius equation. These values give the thermodynamic equilibrium constant (on-enzyme K_{eq}) needed for interpretation of T-jump relaxation kinetic experiments. The on-enzyme K_{eq} values determined for both native and the single-Trp PNP mutant vary by a factor of 20 in the temperature range between 1 and 37 °C (Table 3). While the on-enzyme

Table 3: Comparison of Pre-Steady-State Kinetic Rates (Forward and Reverse)[a] and On-Enzyme K_{eq}[b] for F159W-Leuko- and Native PNPs

	F159W-Leuko-PNP (Ino-HX)			native PNP (Guo-Gua)		
temp, °C	$k_{(chem)f}$, s^{-1}	$k_{(chem)r}$, s^{-1}	K_{eq}	$k_{(chem)f}$, s^{-1}	$k_{(chem)r}$, s^{-1}	K_{eq}
1	75	7	11.2	9	39	0.23
3	79	9	8.8	12	42	0.28
5	83	10	8	15	44	0.34
8	100	18	5.4	22	49	0.44
11	115	26	4.4	31	54	0.57
15	135	44	3.0	50	61	0.81
20	175	82	2.12	89	71	1.25
25	209	152 (108 ± 30)[c]	1.4	154	80	1.92
30	255	275	0.93	262	93	2.81
37	334	608	0.55	536	111	4.82

[a] Determined by stopped-flow fluorescent studies (in the temperature range between 1 and 20 °C or extrapolated from the Arrhenius equation above this temperature range) for F159W-Leuko-PNP with inosine/hypoxanthine and native PNP with guanosine/guanine as substrates for the forward (f) and reverse (r) reactions, respectively. [b] Calculated from the ratio between $k_{(chem)f}$ and $k_{(chem.)r}$. [c] Determined at room temperature (22 °C) by quench flow for F159W-Leuko-PNP with hypoxanthine and ribose 1-phosphate.

Table 4: Comparison of the Thermodynamic Parameters of F159W-Leuko- and Native PNPs at 25 °C

	F159W-Leuko-PNP (Ino-HX)		native PNP (Guo-Gua)	
parameter[a]	forward	reverse	forward	reverse
$k_{(chem)}$, s^{-1}	209 ± 2	152 ± 3	154 ± 3	80 ± 2
$\Delta H^{\ddagger}$, kJ mol^{-1}	28 ± 2	86 ± 6	78 ± 3	18 ± 1
$T\Delta S^{\ddagger}$, kJ mol^{-1}	−32 ± 2	26 ± 2	17 ± 1	−44 ± 2
$\Delta G^{\ddagger}$, kJ mol^{-1}	60 ± 5	60 ± 6	60 ± 4	62 ± 4
$E_a^{\ddagger}$, kJ mol^{-1}	30 ± 2	88 ± 6	80 ± 3	20 ± 0.5

[a] Determined by fitting the stopped-flow fluorescence rates to the Arrhenius (eq 3) and the Eyring (eq 4) equations.

K_{eq} increases with increasing temperature for the native PNP reaction with guanosine, it decreases for the F159W-Leuko-PNP reaction with inosine. Differences between F159-Leuko-PNP and native PNP are most likely attributed to altered interactions at the catalytic sites. This temperature dependence of the thermodynamic equilibrium constants is consistent with large enthalpic components for both enzymes with both substrates. The magnitude of on-enzyme K_{eq} variation for the single Trp mutant as a function of temperature was twice as much as for native enzyme (Table 3), making F159W-Leuko-PNP a better subject for fluorescent T-jump relaxation kinetics. F159W-Leuko-PNP also has an equilibrium constant near unity in the temperature range between 20 and 30 °C, making it a favorable candidate for T-jump analyses.

Analysis of the temperature dependencies of the forward and the reverse catalytic turnover numbers (k_4 and k_{-4}, Scheme 2) according to the Arrhenius and Eyring equations for native (*49*) or single Trp mutant PNPs showed linear increases of the ln(k) or ln(k/T) values with increasing temperature (Figure 3). Different activation enthalpies ($\Delta H^{\ddagger}$) and activation entropies ($\Delta S^{\ddagger}$) were determined for both enzymes with substrates in the forward and reverse directions of the chemical reaction (Table 4). At 25 °C, the activation enthalpy ($\Delta H^{\ddagger}$), the activation entropy ($T\Delta S^{\ddagger}$), and the activation energy (E_a) of the reverse chemical reaction for F159W-Leuko-PNP was increased compared to those for the forward reaction (Table 4). In this case, the increase in activation entropy compensated for the high energy barrier ($\Delta H^{\ddagger}$ and E_a) of the reverse reaction (*55*−*58*). In contrast,

an increase of the activation enthalpy ($\Delta H^{\ddagger}$), the activation entropy ($T\Delta S^{\ddagger}$), and the activation energy (E_a) for the forward chemical reaction compared to that for the reverse reaction was observed for native PNP (Table 4). With native PNP, the activation entropy increased to compensate for the high enthalpic barrier ($\Delta H^{\ddagger}$ and E_a) of the forward reaction (*55*−*58*). Dynamic freedom of the substrate within the enzyme active site, the degree of freedom of the catalytic site residues, and solvent reorganization all contribute to the activation entropy (*59, 60*). The entropic contributions are most likely to result from altered system dynamics leading to transition-state formation for the reverse and forward reaction catalyzed by F159W-Leuko-PNP and native PNP, respectively (*59*−*63*). Differences between F159-Leuko-PNP and native PNP are probably due to altered flexibility at the catalytic sites.

Association and Dissociation Binding Rates. The association and dissociation rates for hypoxanthine binding to F159W-Leuko-PNP-PO_4 were determined by stopped-flow fluorometry. The rates of hypoxanthine association and the formation of F159W-Leuko-PNP-Hx-PO_4 complexes increased monotonically with increasing temperature (Figure 3C). The rate of hypoxanthine association (k_{on}) to F159W-Leuko-PNP-PO_4 at 25 °C was determined to be (1.2 ± 0.1) × 10^7 M^{-1} s^{-1} and with a calculated dissociation rate (k_{off}) of 178 ± 8 s^{-1} (K_d = 15 μM). The association and dissociation rates for guanine binding to Leuko-PNP-PO_4 were previously determined by stopped-flow fluorometry (k_{on} and k_{off} values of 2.7 ± 0.1 × 10^7 M^{-1} s^{-1} and 86 ± 8 s^{-1}, respectively) and T-jump relaxation kinetics (k_{on} and k_{off} values of (3.6 ± 0.2) × 10^7 M^{-1} s^{-1} and 142 ± 36 s^{-1}, respectively) (*38*). The ~2-fold differences in association or dissociation rates between F159W-Leuko-PNP with hypoxanthine and Leuko-PNP with guanine are consistent with slower association, and the faster dissociation rates of hypoxanthine may be due to increased steric effects from the indole ring of W159 as compared to F159 in the parent enzyme.

T-Jump Relaxation Kinetics. Laser-induced T-jump (10−18, 20−27, and 25−32 °C) fluorescence relaxation profiles of equilibrated F159W-Leuko-PNP-inosine-PO_4 ↔ F159W-Leuko-PNP-hypoxanthine-ribose 1-phosphate and the F159W-Leuko-PNP-hypoxanthine-PO_4 ternary complex showed at least four exponential relaxations with time constants of ~0.1−1 μs for τ_1, ~1−100 μs for τ_2, ~100−1000 μs for τ_3, and ~1000−10000 μs for τ_4 (Figures 4 and 5). It was difficult to unambiguously assign the fluorescence relaxation kinetic rates for τ_1 and τ_4. τ_1 is most likely to represent substrate (inosine or hypoxanthine) binding to PNP, but the weak signal-to-noise ratio did not allow accurate experimental determination at this fast time scale (~0.1−1 μs). Rates for guanine association ((3.6 ± 0.2) × 10^7 M^{-1} s^{-1}) and dissociation (142 ± 36 s^{-1}) from the Leuko-PNP-PO_4 complex were previously determined using T-jump relaxation kinetics (*38*). For τ_4 (k_4 and k_{-4}), the 1−15 ms relaxation time scale overlapped the cooling time range for this instrumentation, preventing the unequivocal experimental determination of this relaxation time. However, constants in the millisecond time scale are readily accessible using stopped-flow fluorescence techniques. The microscopic rate constants k_2, k_{-2}, k_3, and k_{-3} for conformational changes of F159W-leuko-PNP (Scheme 2) were obtained directly by fitting the well-resolved T-jump relaxation times τ_2^{-1} and τ_3^{-1} to eqs 5 and 6, respectively (*47, 64*) (Figures 4 and 5, Table 5). The F159W-Leuko-PNP Trp reporter shows excellent signal-to-noise ratio and kinetic resolution for protein conformational changes in the nanosecond to millisecond time scale (τ_2 and τ_3). Relaxation kinetic rates of ~10500, 2200, 1500, and 900 s^{-1} were determined at 25 °C for the active equilibrium of F159W-Leuko-PNP-inosine-PO_4 ↔ F159W-Leuko-PNP-hypoxanthine-ribose 1-phosphate based on fluorescent changes as a function of T-jump and reactant concentrations. These rates can be compared to those of 11100, 2700, 1300, and 200 s^{-1} for the dead-end ternary complex of F159W-Leuko-PNP-hypoxanthine-PO_4 (Table 6). The 900 s^{-1} relaxation rate is therefore related to inosine but not hypoxanthine active site interactions. The 200 s^{-1} relaxation rate specific to the nonreactive ternary complex is likely to be a conformational change related to both Trp159 movement, giving the spectral change, and catalysis since the on-enzyme catalytic turnover rates are 209 s^{-1} and 152 s^{-1} for k_4 ($k_{(chem)f}$) and k_{-4} ($k_{(chem)r}$), respectively, at 25 °C (Table 6). The experimentally determined constants (τ_2^{-1} and τ_3^{-1}) are much faster than catalysis and are proposed to represent binding, loop motions, domain changes, and residue alignments that are preludes to the relatively long (~5 ms) dynamic search required to form the transition state.

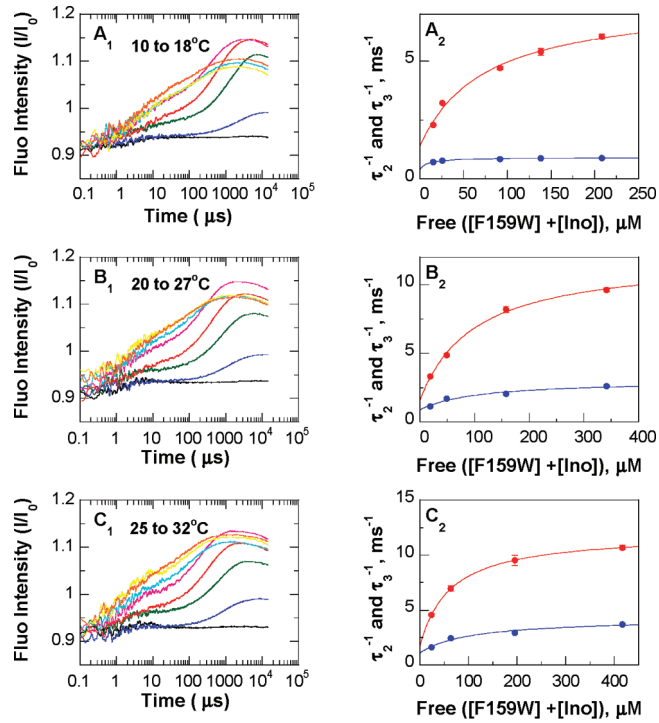

FIGURE 4: T-jump relaxation kinetics of F159W-Leuko-PNP-inosine-PO_4 ↔ F159W-Leuko-PNP-hypoxanthine-ribose 1-phosphate equilibrated system. Panels A_1, B_1, and C_1: T-jump fluorescence relaxation traces at different concentrations of inosine (black, blue, green, red, pink, light blue, yellow, and orange traces were recorded at 0, 13, 32, 80, 160, 400, 560, and 800 μM inosine, respectively) as a function of time (μs). Panels A_2, B_2, and C_2: Fluorescence relaxation rates [τ_2^{-1} (red dot) and τ_3^{-1} (blue dot)] determined from the fluorescence relaxation traces in the corresponding panels (A_1, B_1, and C_1, respectively) as a function of free enzyme and inosine concentrations; red and blue lines are a fit of the data to eqs 5 and 6, respectively. Temperature jumps were from 10 to 18 °C (panels A), 20 to 27 °C (panels B), and 25 to 32 °C (panels C). In curve fitting, the cooling process (>1 ms) was accounted for by a separate relaxation component with fixed time constant determined from temperature profiles.

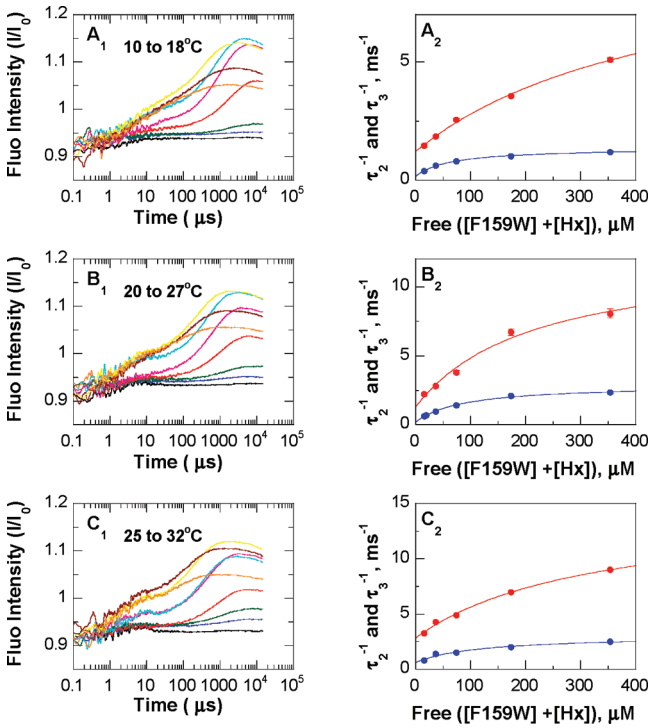

FIGURE 5: T-jump relaxation kinetics of the F159W-Leuko-PNP-hypoxanthine-PO_4 ternary complex equilibrated system. Panels A_1, B_1, and C_1: T-jump fluorescence relaxation traces at different concentrations of hypoxanthine (black, blue, green, red, pink, light blue, yellow, dark red, and orange traces were recorded at 0, 5.7, 12, 28, 60, 100, 200, 381, and 798 μM hypoxanthine, respectively) as a function of time (μs). Panels A_2, B_2, and C_2: Fluorescence relaxations rates [τ_2^{-1} (red dot) and τ_3^{-1} (blue dot)] determined from the fluorescence relaxation traces in the corresponding panels (A_1, B_1, and C_1, respectively) as a function of free enzyme and hypoxanthine concentrations; red and blue lines are a fit of the data to eqs 5 and 6, respectively. Temperature jumps were from 10 to 18 °C (panels A), 20 to 27 °C (panels B), and 25 to 32 °C (panels C). In curve fitting, the cooling process (>1 ms) was accounted for by a separate relaxation component with fixed time constant determined from temperature profiles.

Table 5: Comparison of T-Jump Rate Constants for the Equilibrated Systems of F159W-Leuko-PNP with (a) Inosine-PO_4-Hypoxanthine-Ribose 1-Phosphate and (b) Hypoxanthine-PO_4

temp jump, °C	equilibrated system	τ_2^{-1}, ms^{-1}		τ_3^{-1}, ms^{-1}	
		k_2^a	k_{-2}^a	k_3^b	k_{-3}^b
10−18	a	6.2 ± 0.6	1.4 ± 0.6	0.50 ± 0.17	0.4 ± 0.2
	b	9.0 ± 1.6	1.2 ± 0.1	1.20 ± 0.04	0.2 ± 0.1
20−27	a	10.5 ± 0.6	1.5 ± 0.6	2.2 ± 0.5	0.9 ± 0.5
	b	11.1 ± 2.2	1.3 ± 0.6	2.7 ± 0.1	0.2 ± 0.1
25−32	a	10.3 ± 0.1	1.7 ± 0.1	3.1 ± 0.6	1.1 ± 0.7
	b	11.8 ± 2.0	2.8 ± 0.3	2.4 ± 0.4	0.6 ± 0.3

[a] Determined by fitting the relaxation rate (τ_2^{-1}) to eq 5. [b] Determined by fitting the relaxation rate (τ_3^{-1}) to eq 6.

Thermodynamics of F159W-Leuko-PNP. The on-enzyme equilibrium for native and F159W-Leuko-PNP differs, but both show strong temperature dependence, indicating a substantial enthalpic component to the on-enzyme chemical equilibria (Table 3). Quantitation of these differences show equivalent $\Delta G^{\ddagger}$ values for native and F159W-Leuko-PNP but substantial differences in $\Delta H^{\ddagger}$ values and $T\Delta S^{\ddagger}$ values (Table 4). Transition-state analysis of human PNP mutants with amino acid changes remote from the catalytic site have indicated that the full dynamic structure of the protein can influence transition-state structure (*14, 51*). With F159W-Leuko-PNP, at 25 °C, the conversion of bound inosine and phosphate to the transition state is almost equally distributed into enthalpic and entropic components (Figure 6). With equivalent $\Delta G^{\ddagger}$ values for forward and reverse reactions the K_{eq} is near unity at this temperature. The reverse reaction of enzyme-bound hypoxanthine and ribose 1-phosphate is dominated by the enthalpic component by 3-fold compared to the $T\Delta S^{\ddagger}$ value.

Table 6: Summary of Microscopic Rate Constants (Scheme 2) for the Two Equilibrated Systems of F159W-Leuko-PNP at 25 °C

microscopic rates	F159W-Leuko-PNP-Ino-PO_4-Hx-R1PO_4	F159W-Leuko-PNP-Hx-PO_4
k_1, M^{-1} s^{-1}	(1.2 ± 0.1) × 10^7	
k_{-1}, s^{-1}	178 ± 8	
k_2, s^{-1}	10500 ± 600	11100 ± 2200
k_{-2}, s^{-1}	1500 ± 600	1300 ± 600
k_3, s^{-1}	2200 ± 500	2700 ± 100
k_{-3}, s^{-1}	900 ± 500	200 ± 100
k_4, s^{-1}	209 ± 2	na[a]
k_{-4}, s^{-1}	152 ± 3	na[a]

[a] Not available.

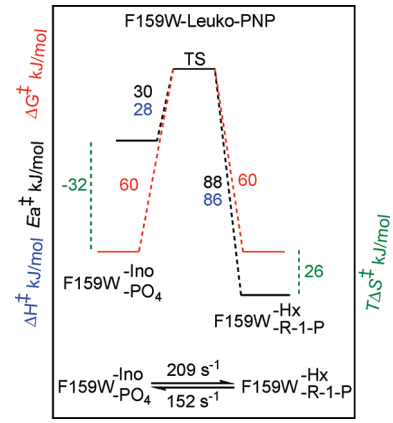

FIGURE 6

T-Jump Relaxations. T-Jump experiments with increasing concentrations of enzyme, inosine, hypoxanthine, and phosphate are capable of distinguishing time-resolved species and first-order from higher order reactions (Figures 4 and 5 and Scheme 2). At high concentrations of inosine and phosphate, the enzyme exists in an equilibrating mixture of fully saturated forms (Figure 6). Altered environments of W159 are seen, with increased fluorescence intensity for the inosine or free enzyme complexes and quenched fluorescence with the complexes bound with hypoxanthine (Figure 2). Over the titrations and T-jumps with equilibrated enzyme, inosine, and phosphate, three relaxations are resolved (Figure 4 and Table 6). Rate constants k_4 and k_{-4} were established with stopped-flow studies and are the chemical step for enzyme-bound reagents (Scheme 2 and Table 4). Three of the rate constants associated with steps k_2, k_{-2}, k_3, and k_{-3} are faster than the chemical steps (k_4 and k_{-4} in Scheme 2a), but the constants at 200 s^{-1} in both Scheme 2a and Scheme 2b are the same as the rate of chemical conversion of enzyme-bound inosine to enzyme-bound hypoxanthine. In the presence of the fully equilibrating catalytic reaction, this rate can be reasonably assigned to chemistry and, in the enzyme saturated with only hypoxanthine and phosphate, to a change in W159 linked to catalysis.

The physiological reaction of PNP involves inosine binding to the enzyme−phosphate complex (Scheme 2a) followed by two time-resolved conformational changes with forward and reverse first-order rate constants from 900 to 10500 s^{-1}. As these must influence W159 to give the observed fluorescent changes, two of these constants involve closing and opening of the W159 loop that covers the catalytic site, and the second pair of constants can be proposed to be the catalytic site reorganization in response to catalytic site closing. A comparison of the substrate analogue complexes with transition-state analogues bound at the catalytic site of bovine PNP indicates that as many as six new H-bonds form in the tightly bound transition-state complex (*65*). The dynamic approach to transition-state formation based on the W159 fluorescent probe can be summarized as (1) substrate binding at $\sim 1.2 \times 10^7$ M^{-1} s^{-1}, (2) W159 loop closing at 900−10500 s^{-1}, (3) a conformational change that forms a reactant environment providing access to the transition state with a similar time constant, (4) a dynamic search lasting for reciprocal 210 s^{-1} that forms the transition state, and (5) relaxation of the system to release products at a rate of 22 s^{-1}. Computational analysis by transition path sampling for human PNP indicates a transition-state lifetime of 10 fs (*17*), emphasizing that transition-state lifetime is extremely short relative to the protein conformational dynamics probed by spectroscopic techniques. Only local dynamic motion (side chain atomic vibrations) is coupled to the transition-state lifetime, and the conformations observed on the nanosecond to millisecond time scale are relatively static preequilibrated states relative to the lifetime of the transition state.

CONCLUSION

F159W-Leuko-PNP provides a reporter group for catalytic site geometry changes associated with on-enzyme ligand binding, conformational changes, and chemistry. T-jump analysis of enzyme complexes establishes a minimum of four distinct structural states for the enzyme saturated with substrates and products. Product release is rate limiting for PNPs (*49, 66*) (22 s^{-1} at 25 °C for F159W-Leuko-PNP), and the rate of chemical conversion at the catalytic site is ~5 ms at 25 °C. In a dynamic interpretation of catalysis, this time involves a dynamic search to optimize the catalytic site geometry needed to cross the transition-state barrier. Promoting vibrations exemplified by the O5′−O4′ compression mode associated with catalysis occur on the ~30 fs time scale (*17*); therefore $\sim 1.6 \times 10^{11}$ such excursions occur on average to cross the transition-state barrier. T-jump analysis of F159W-Leuko-PNP establishes multiple protein conformational changes influencing the fluorescence of W159 that occur on the nanosecond to millisecond time scale as the enzyme organizes to place catalytic site groups close to the positions from which catalysis occurs. Based on the extreme differences in time scales between the promoting vibrations (~30 fs) linked directly to transition-state formation and the short lifetime of the transition state (10 fs), the states detected by fluorescence changes of F159W-Leuko-PNP demonstrate multiple time-resolved conformational changes in PNP that are relatively stable states on the time scale of transition-state formation. These are proposed to organize catalytic site groups to provide access for the more rapid motions involved in transition-state formation. Formation of the Michaelis complex is followed by conformational changes which are fast on the time scale of catalytic turnover but slow compared to the lifetime of the transition state. The precise protein motions that occur during these conformational changes and the relevance of these motions to the pathway to the transition state remain to be determined.

REFERENCES

1. Giblett, E. R., Ammann, A. J., Wara, D. W., Sandman, R., and Diamond, L. K. (1975) Nucleoside-phosphorylase deficiency in a child with severely defective T-cell immunity and normal B-cell immunity. *Lancet 1*, 1010–1013.
2. Krenitsky, T. A., Tuttle, J. V., Koszalka, G. W., Chen, I. S., Beacham, L. M., III, Rideout, J. L., and Elion, G. B. (1976) Deoxycytidine kinase from calf thymus. Substrate and inhibitor specificity. *J. Biol. Chem. 251*, 4055–4061.
3. Mitchell, B. S., Mejias, E., Daddona, P. E., and Kelley, W. N. (1978) Purinogenic immunodeficiency diseases: selective toxicity of deoxyribonucleosides for T cells. *Proc. Natl. Acad. Sci. U.S.A. 75*, 5011–5014.
4. Núñez, S., Wing, C., Antoniou, D., Schramm, V. L., and Schwartz, S. D. (2006) Insight into catalytically relevant correlated motions in human purine nucleoside phosphorylase. *J. Phys. Chem. A 110*, 463–472.
5. Stoeckler, J. D., Cambor, C., and Parks, R. E., Jr. (1980) Human erythrocytic purine nucleoside phosphorylase: reaction with sugar-modified nucleoside substrates. *Biochemistry 19*, 102–107.
6. Ullman, B. , Gudas, L. J. , Clift, S. M., and Martin, D. W., Jr. (1979) Isolation and characterization of purine-nucleoside phosphorylase-deficient T-lymphoma cells and secondary mutants with altered ribonucleotide reductase: genetic model for immunodeficiency disease. *Proc. Natl. Acad. Sci. U.S.A. 76*, 1074–1078.
7. Duvic, M., Olsen, E. A., Omura, G. A., Maize, J. C., Vonderheid, E. C., Elmets, C. A., Shupack, J. L., Demierre, M. F., Kuzel, T. M., and Sanders, D. Y. (2001) A phase III, randomized, double-blind, placebo-controlled study of peldesine (BCX-34) cream as topical therapy for cutaneous T-cell lymphoma. *J. Am. Acad. Dermatol. 44*, 940–947.
8. Ealick, S. E., Babu, Y. S., Bugg, C. E., Erion, M. D., Guida, W. C., Montgomery, J. A., and Secrist, J. A., III (1991) Application of crystallographic and modeling methods in the design of purine nucleoside phosphorylase inhibitors. *Proc. Natl. Acad. Sci. U.S.A. 88*, 11540–11544.
9. Schramm, V. L. (2002) Development of transition state analogues of purine nucleoside phosphorylase as anti-T-cell agents. *Biochim. Biophys. Acta 1587*, 107–117.
10. De Azevedo, W. F., Jr., Canduri, F., dos Santos, D. M., Silva, R. G., de Oliveira, J. S., de Carvalho, L. P., Basso, L. A., Mendes, M. A., Palma, M. S., and Santos, D. S. (2003) Crystal structure of human purine nucleoside phosphorylase at 2.3Å resolution. *Biochem. Biophys. Res. Commun. 308*, 545–552.
11. Koellner, G., Luic, M., Shugar, D., Saenger, W., and Bzowska, A. (1997) Crystal structure of calf spleen purine nucleoside phosphorylase in a complex with hypoxanthine at 2.15 Å resolution. *J. Mol. Biol. 265*, 202–216.
12. Rinaldo-Matthis, A., Murkin, A. S., Ramagopal, U. A., Clinch, K., Mee, S. P., Evans, G. B., Tyler, P. C., Furneaux, R. H., Almo, S. C., and Schramm, V. L. (2008) L-Enantiomers of transition state analogue inhibitors bound to human purine nucleoside phosphorylase. *J. Am. Chem. Soc. 130*, 842–844.
13. Shi, W., Ting, L. M., Kicska, G. A., Lewandowicz, A., Tyler, P. C., Evans, G. B., Furneaux, R. H., Kim, K., Almo, S. C., and Schramm, V. L. (2004) Plasmodium falciparum purine nucleoside phosphorylase: crystal structures, immucillin inhibitors, and dual catalytic function. *J. Biol. Chem. 279*, 18103–18106.
14. Saen-Oon, S., Ghanem, M., Schramm, V. L., and Schwartz, S. D. (2008) Remote mutations and active site dynamics correlate with catalytic properties of purine nucleoside phosphorylase. *Biophys. J. 94*, 4078–4088.
15. Antoniou, D., Basner, J., Nunez, S., and Schwartz, S. D. (2006) Computational and theoretical methods to explore the relation between enzyme dynamics and catalysis. *Chem. Rev. 106*, 3170–3187.

16. Hammes, G. G. (2002) Multiple conformational changes in enzyme catalysis. *Biochemistry 41*, 8221–8228.
17. Saen-Oon, S., Quaytman-Machleder, S., Schramm, V. L., and Schwartz, S. D. (2008) Atomic detail of chemical transformation at the transition state of an enzymatic reaction. *Proc. Natl. Acad. Sci. U.S.A. 105*, 16543–16548.
18. Schramm, V. L. (2005) Enzymatic transition states and transition state analogues. *Curr. Opin. Struct. Biol. 15*, 604–613.
19. Boehr, D. D., Dyson, H. J., and Wright, P. E. (2006) An NMR perspective on enzyme dynamics. *Chem. Rev. 106*, 3055–3079.
20. Boehr, D. D., McElheny, D., Dyson, H. J., and Wright, P. E. (2006) The dynamic energy landscape of dihydrofolate reductase catalysis. *Science 313*, 1638–1642.
21. Eisenmesser, E. Z., Millet, O., Labeikovsky, W., Korzhnev, D. M., Wolf-Watz, M., Bosco, D. A., Skalicky, J. J., Kay, L. E., and Kern, D. (2005) Intrinsic dynamics of an enzyme underlies catalysis. *Nature 438*, 117–121.
22. Johnson, E., Palmer, A. G., III, and Rance, M. (2007) Temperature dependence of the NMR generalized order parameter. *Proteins 66*, 796–803.
23. Kern, D., Eisenmesser, E. Z., and Wolf-Watz, M. (2005) Enzyme dynamics during catalysis measured by NMR spectroscopy. *Methods Enzymol. 394*, 507–524.
24. Massi, F., and Palmer, A. G., III (2003) Temperature dependence of NMR order parameters and protein dynamics. *J. Am. Chem. Soc. 125*, 11158–11159.
25. Massi, F., Wang, C., and Palmer, A. G., III (2006) Solution NMR and computer simulation studies of active site loop motion in triosephosphate isomerase. *Biochemistry 45*, 10787–10794.
26. Palmer, A. G., III (2004) NMR characterization of the dynamics of biomacromolecules. *Chem. Rev. 104*, 3623–3640.
27. Brewer, S. H., Song, B., Raleigh, D. P., and Dyer, R. B. (2007) Residue specific resolution of protein folding dynamics using isotope-edited infrared temperature jump spectroscopy. *Biochemistry 46*, 3279–3285.
28. Desamero, R., Rozovsky, S., Zhadin, N., McDermott, A., and Callender, R. (2003) Active site loop motion in triosephosphate isomerase: T-jump relaxation spectroscopy of thermal activation. *Biochemistry 42*, 2941–2951.
29. Khajehpour, M., Wu, L., Liu, S., Zhadin, N., Zhang, Z. Y., and Callender, R. (2007) Loop dynamics and ligand binding kinetics in the reaction catalyzed by the *Yersinia* protein tyrosine phosphatase. *Biochemistry 46*, 4370–4378.
30. McClendon, S., Vu, D. M., Clinch, K., Callender, R., and Dyer, R. B. (2005) Structural transformations in the dynamics of Michaelis complex formation in lactate dehydrogenase. *Biophys. J. 89*, L07−09.
31. McClendon, S., Zhadin, N., and Callender, R. (2005) The approach to the Michaelis complex in lactate dehydrogenase: the substrate binding pathway. *Biophys. J. 89*, 2024–2032.
32. Callender, R., and Dyer, R. B. (2006) Advances in time-resolved approaches to characterize the dynamical nature of enzymatic catalysis. *Chem. Rev. 106*, 3031–3042.
33. Zhadin, N., Gulotta, M., and Callender, R. (2008) Probing the role of dynamics in hydride transfer catalyzed by lactate dehydrogenase. *Biophys. J. 95*, 1974–1984.
34. Crehuet, R., and Field, M. J. (2007) A transition path sampling study of the reaction catalyzed by the enzyme chorismate mutase. *J. Phys. Chem. B 111*, 5708–5718.
35. Gao, J., Major, D. T., Fan, Y., Lin, Y. L., Ma, S., and Wong, K. Y. (2008) Hybrid quantum and classical methods for computing kinetic isotope effects of chemical reactions in solutions and in enzymes. *Methods Mol. Biol. 443*, 37–62.
36. Quaytman, S. L., and Schwartz, S. D. (2007) Reaction coordinate of an enzymatic reaction revealed by transition path sampling. *Proc. Natl. Acad. Sci. U.S.A. 104*, 12253–12258.
37. Jimenez, A., Clapes, P., and Crehuet, R. (2008) A dynamic view of enzyme catalysis. *J. Mol. Model. 14*, 735–746.
38. Ghanem, M., Saen-oon, S., Zhadin, N., Wing, C., Cahill, S. M., Schwartz, S. D., Callender, R., and Schramm, V. L. (2008) Tryptophan-free human PNP reveals catalytic site interactions. *Biochemistry 47*, 3202–3215.
39. Lewandowicz, A., and Schramm, V. L. (2004) Transition state analysis for human and *Plasmodium falciparum* purine nucleoside phosphorylases. *Biochemistry 43*, 1458–1468.
40. Kim, B. K., Cha, S., and Parks, R. E., Jr. (1968) Purine nucleoside phosphorylase from human erythroyctes. II. Kinetic analysis and substrate-binding studies. *J. Biol. Chem. 243*, 1771–1776.
41. Lewandowicz, A., Shi, W., Evans, G. B., Tyler, P. C., Furneaux, R. H., Basso, L. A., Santos, D. S., Almo, S. C., and Schramm, V. L. (2003) Over-the-barrier transition state analogues and crystal structure with *Mycobacterium tuberculosis* purine nucleoside phosphorylase. *Biochemistry 42*, 6057–6066.
42. Kicska, G. A., Tyler, P. C., Evans, G. B., Furneaux, R. H., Kim, K., and Schramm, V. L. (2002) Transition state analogue inhibitors of purine nucleoside phosphorylase from *Plasmodium falciparum*. *J. Biol. Chem. 277*, 3219–3225.
43. Rinaldo-Matthis, A., Wing, C., Ghanem, M., Deng, H., Wu, P., Gupta, A., Tyler, P. C., Evans, G. B., Furneaux, R. H., Almo, S. C., Wang, C. C., and Schramm, V. L. (2007) Inhibition and structure of *Trichomonas vaginalis* purine nucleoside phosphorylase with picomolar transition state analogues. *Biochemistry 46*, 659–668.
44. Miles, R. W., Tyler, P. C., Furneaux, R. H., Bagdassarian, C. K., and Schramm, V. L. (1998) One-third-the-sites transition-state inhibitors for purine nucleoside phosphorylase. *Biochemistry 37*, 8615–8621.
45. Singh, V., Evans, G. B., Lenz, D. H., Mason, J. M., Clinch, K., Mee, S., Painter, G. F., Tyler, P. C., Furneaux, R. H., Lee, J. E., Howell, P. L., and Schramm, V. L. (2005) Femtomolar transition state analogue inhibitors of 5′-methylthioadenosine/S-adenosylhomocysteine nucleosidase from *Escherichia coli*. *J. Biol. Chem. 280*, 18265–18273.
46. Dawson, R. M. C., Elliott, D., Elliott, W. H., and Jones, K. M. (1986) Spectral data and pK_a values for purines, pyrimidines, nucleosides, and nucleotides, in *Data for biochemical research*, 3rd ed., pp 103−114, Oxford University Press, New York.
47. Leffler, J. E., and Grunwald, E. (1963) *Rates and Equilibria of Organic Reactions*, pp 77−86, Wiley, New York.
48. Kline, P. C., and Schramm, V. L. (1992) Purine nucleoside phosphorylase. Inosine hydrolysis, tight binding of the hypoxanthine intermediate, and third-the-sites reactivity. *Biochemistry 31*, 5964–5973.
49. Ghanem, M., Li, L., Wing, C., and Schramm, V. L. (2008) Altered thermodynamics from remote mutations altering human toward bovine purine nucleoside phosphorylase. *Biochemistry 47*, 2559–2564.
50. Li, L., Luo, M., Ghanem, M., Taylor, E. A., and Schramm, V. L. (2008) Second-sphere amino acids contribute to transition-state structure in bovine purine nucleoside phosphorylase. *Biochemistry 47*, 2577–2583.
51. Luo, M., Li, L., and Schramm, V. L. (2008) Remote mutations alter transition-state structure of human purine nucleoside phosphorylase. *Biochemistry 47*, 2565–2576.
52. Lakowicz, J. (1999) *Principles of Fluorescence Spectroscopy*, 2nd ed., Kluwer Academic Publishers, Dordrecht, The Netherlands.
53. Vivian, J. T., and Callis, P. R. (2001) Mechanisms of tryptophan fluorescence shifts in proteins. *Biophys. J. 80*, 2093–2109.
54. Assenza, S. P., and Brown, P. R. (1984) Ultraviolet and fluorescence characterization of purines and pyrimidines by post-column pH manipulation. *J. Chromatogr. 289*, 355–365.
55. Sharp, K. (2001) Entropy-enthalpy compensation: fact or artifact? *Protein Sci. 10*, 661–667.
56. Street, T. O., Bradley, C. M., and Barrick, D. (2005) An improved experimental system for determining small folding entropy changes resulting from proline to alanine substitutions. *Protein Sci. 14*, 2429–2435.
57. Vaz, D. C., Rodrigues, J. R., Sebald, W., Dobson, C. M., and Brito, R. M. (2006) Enthalpic and entropic contributions mediate the role of disulfide bonds on the conformational stability of interleukin-4. *Protein Sci. 15*, 33–44.
58. Villa, J., Strajbl, M., Glennon, T. M., Sham, Y. Y., Chu, Z. T., and Warshel, A. (2000) How important are entropic contributions to enzyme catalysis? *Proc. Natl. Acad. Sci. U.S.A. 97*, 11899–11904.
59. Ottosson, J., Fransson, L., and Hult, K. (2002) Substrate entropy in enzyme enantioselectivity: an experimental and molecular modeling study of a lipase. *Protein Sci. 11*, 1462–1471.
60. Ottosson, J., Rotticci-Mulder, J. C., Rotticci, D., and Hult, K. (2001) Rational design of enantioselective enzymes requires considerations of entropy. *Protein Sci. 10*, 1769–1774.
61. Jonsson, W. E., Adlercreutz, P., and Mattiasson, B. (1999) Thermodynamic and kinetic aspects on water vs. organic solvent as reaction media in the enzyme-catalysed reduction of ketones. *Biochim. Biophys. Acta 1430*, 313–322.

62. Verheyden, G., Matrai, J., Volckaert, G., and Engelborghs, Y. (2004) A fluorescence stopped-flow kinetic study of the conformational activation of α-chymotrypsin and several mutants. *Protein Sci. 13*, 2533–2540.
63. Jensen, M. P., Payeras, A. M., Fiedler, A. T., Costas, M., Kaizer, J., Stubna, A., Munck, E., and Que, L., Jr. (2007) Kinetic analysis of the conversion of nonheme (alkylperoxo)iron(III) species to iron(IV) complexes. *Inorg. Chem. 46*, 2398–2408.
64. Hammes, G. G., and Schimmel, P. R. (1970) Rapid reactions and transient states, in *The Enzymes* (Boyer, P. D., Ed.) pp 67−114, Academic Press, New York.
65. Fedorov, A., Shi, W., Kicska, G., Fedorov, E., Tyler, P. C., Furneaux, R. H., Hanson, J. C., Gainsford, G. J., Larese, J. Z., Schramm, V. L., and Almo, S. C. (2001) Transition state structure of purine nucleoside phosphorylase and principles of atomic motion in enzymatic catalysis. *Biochemistry 40*, 853–860.
66. Schramm, V. L. (2005) Enzymatic transition states: thermodynamics, dynamics and analogue design. *Arch. Biochem. Biophys. 433*, 13–26.

BI802339C